Two-Dimensional Radiation Field Map of a Be-based Source

Bachelor Thesis
by Henrik Söderhielm
Supervisor: Dr. Kevin Fissum
Co-Supervisor: Dr. Francesco Messi

Division of Nuclear Physics
Department of Physics
Lund University

HT16
FYSK02

LUND
UNIVERSITY

Abstract

The aim of this project was to measure the profile of the radiation exiting an aperture of the Aquarium at the Source Testing Facility at the Division of Nuclear Physics at Lund University. So far, the outgoing beam of radiation at the aperture of the Aquarium has been assumed to be uniform. The radiation is produced by a Beryllium-based radioactive source and comes in the form of neutrons and γ-rays. Thermal neutrons were detected using a ^{3}He proportional counter and γ-rays were detected using a Cerium-Activated Lanthanum Bromide scintillation detector. To form a two-dimensional map of the radiation, the detectors were placed at several different well-defined positions. The data obtained in the measurements that were performed showed that the intensity of radiation indeed varies across the different positions. The ultimate goal of the project to which this thesis contributes is to create a simulation framework that provides a map of the radiation profile at the aperture of the Aquarium. This will facilitate precision studies of newly developed detector responses in the future.

Abbreviations

ADC	Analog to Digital Converter
AmBe	Americium-Beryllium
CAD	Computer Aided Design
DNPLU	Division of Nuclear Physics at Lund University
ESS	European Spallation Source
^{3}He	Helium-3
$LaBr_3(Ce)$	Cerium-Activated Lanthanum Bromide
MCA	Multi-Channel Analyzer
PMT	Photomultiplier Tube
PuBe	Plutonium-Beryllium
STF	Source Testing Facility

Contents

List of Figures

List of Tables

Chapter 1

Introduction

Neutrons are valuable to the field of material research. As they carry no electrical charge, they easily penetrate matter. They are therefore useful for non-invasive investigations. The European Spallation Source (ESS), which is under construction in Lund, Sweden, will soon lie at the forefront of global neutron research. The ability to detect neutrons is paramount to ESS and detection methods for neutrons are constantly evolving. The Division of Nuclear Physics at Lund University (DNPLU) is home to the Source Testing Facility (STF). The STF hosts the Aquarium, an infrastructure which, together with radioactive sources, provides a platform for the development of neutron detectors.

The radiation studied in this thesis comes in two different forms: photons and neutrons. Photons are massless elementary particles described by quantum physics. The highly energetic photons considered in this thesis are called γ-rays. γ-rays have energies over 100 keV. Neutrons are particles that along with protons make up the nucleus of an atom. Their properties are described by nuclear physics. The neutrons considered in this thesis are called thermal neutrons. Thermal neutrons have a very low kinetic energy of about 0.025 eV. γ-rays and neutrons interact with matter in completely different ways. γ-rays interact primarily with atomic electrons while neutrons interact with atomic nuclei via scattering and nuclear reactions. This necessitates the need for two different types of radiation detectors. In this thesis, γ-rays were detected with a $LaBr_3$(Ce) crystal and thermal neutrons were detected with a ^{3}He proportional counter.

The Aquarium houses the Be-based source used in this work. The radiation from the source is emitted isotropically. The water in the Aquarium is used to shield the outside world from this radiation. Ideally, there should not be any additional radiation emitted to the world outside of the Aquarium due to the source, and neutrons and γ-rays should only exit in a controlled fashion from penetrations in the shielding. Furthermore, the radiation field at the apertures of the Aquarium should be uniform.

The work presented in this thesis involved mapping the variation in intensity of the radiation at different positions in and around an Aquarium aperture. The results of this project provide a visualization of the radiation field at the Aquarium apertures. Knowledge of the behavior of this field will allow for future unfolding from measured detector responses, facilitating precise knowledge of detector-response functions.

Chapter 2

Method

2.1 Experimental Setup

The experiment involved placing detectors in front of an aperture of the Aquarium in order to detect outgoing radiation from the Be-based source placed at its center. The detectors were placed at ten well-defined positions to produce contour maps of the outgoing radiation. Measurements were then performed.

2.1.1 The Aquarium

The STF at the DNPLU hosts the Aquarium shown in Fig. 2.1. The Aquarium is a tank of water with a central void in which a radioactive source may be placed. Four circular apertures, one on each side and each with a diameter of 19 cm, define a direct beam of radiation from the source. The purpose of the Aquarium apertures (tunnels) is to limit the divergence of the radiation. The apertures act as waveguides and ideally result a uniform beams of γ-rays and neutrons [1].

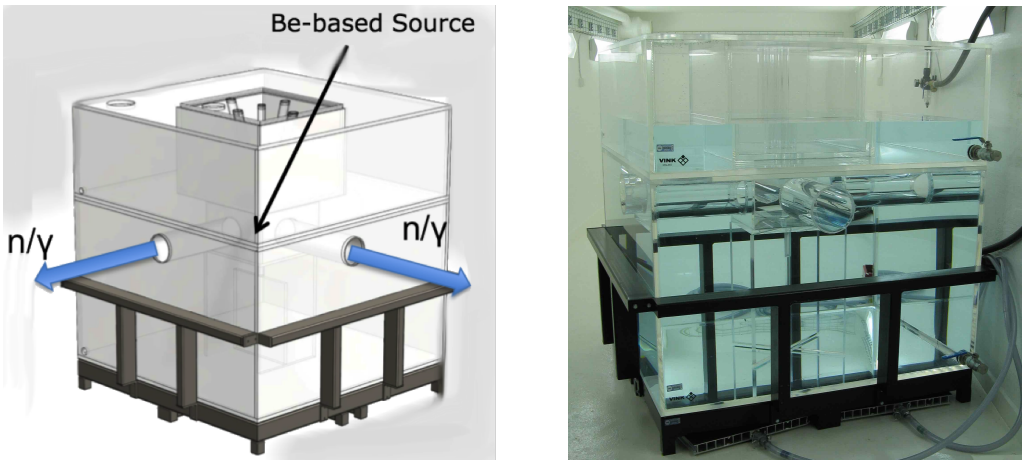

Figure 2.1: Left: CAD of the Aquarium in the STF [2]. Right: The Aquarium in the STF [1].

2.1.2 Beryllium-Based Source

Neutrons are produced in a Be-based source through actinide[1]-induced reactions. Actinides such as Plutonium or Americium decay through α-emission. The α-particle then

[1]Heavy elements with atomic number 89-103.

interacts with Beryllium via the following reactions:

$$\alpha + {}^{9}\mathrm{Be} \rightarrow \begin{cases} {}^{12}\mathrm{C} + n & \text{(ground state)} \\ {}^{12}\mathrm{C}^{*} + n & \text{(first excited state) at 4.44 MeV} \\ {}^{12}\mathrm{C}^{**} + n & \text{(second excited state) at 7.16 MeV} \end{cases} \tag{2.1}$$

When ^{12}C is produced in its ground state, the Q-value[2] of this exothermic reaction is 5.7 MeV. The Q-value can be calculated according to:

$$Q = m_{^{9}\mathrm{Be}} + m_{\alpha} - m_{n} - m_{^{12}\mathrm{C}}, \tag{2.2}$$

where $m_{^{9}\mathrm{Be}}$ is the mass of ^{9}Be, m_{α} is the mass of the alpha particle, m_{n} is the neutron mass and $m_{^{12}\mathrm{C}}$ is the mass of ^{12}C. In reactions where the first excited state of ^{12}C results, the excited nucleus decays by emission of a 4.44 MeV γ-ray [3]. It is this reaction that was exploited in this work. The reaction involving the second excited state of ^{12}C was not accessible. Figure 2.2 shows a picture of the source that was used for the experiment. The source used for the measurements is a Plutonium-Beryllium mixed field γ-ray and neutron source (PuBe).

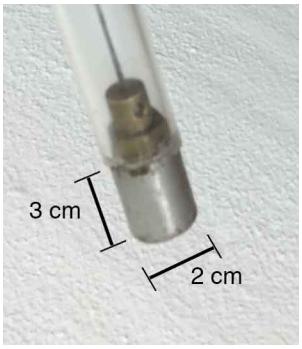

Figure 2.2: The PuBe source used in this thesis.

2.1.3 Detector Platform

To obtain accurate results, a stable placement for the detectors was required. The first challenge was to build a platform for the detectors that is adjustable between well-defined positions.

$LaBr_3$(Ce), ^{3}He Detector Platform

For the lightweight ^{3}He and $LaBr_3$(Ce) detectors, a structure built out of foamcore boards and strong glue sufficed. It was a design made of inexpensive materials which provide a sufficiently precise positioning of virtually any detector that fits the platform. Additionally, positioning is reproducible. Figure 2.3 illustrates the basic concept of the platform. The detector was held between pillars from which its position could be adjusted vertically. These pillars were in turn built on another platform which could be shifted horizontally. The fixed positions were clearly marked on the base platform. The platform was simply taped to a height-adjustable table and the vertically lowest and horizontally central positions were aligned with the bottom of the Aquarium aperture as shown in the previous section. See also Fig. 2.7.

[2]The energy released in the reaction.

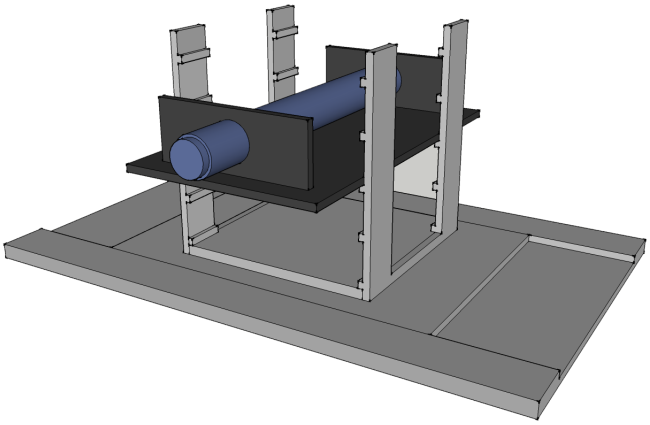

Figure 2.3: A CAD visualization of the detector platform.

Figure 2.4 shows how the $LaBr_3(Ce)$ and ^3He detectors were positioned on the platform. The photographs demonstrate the direction the detectors were facing during the experiment.

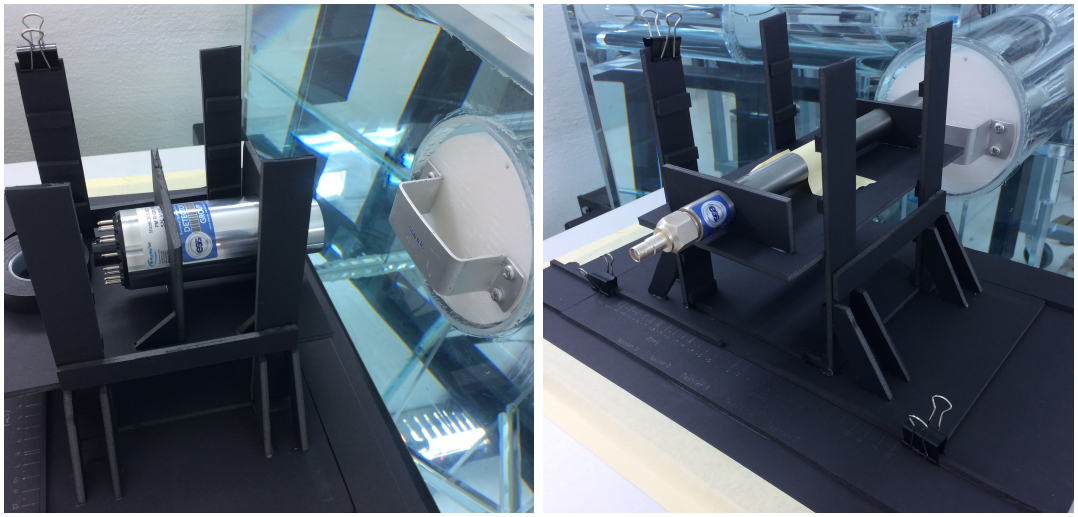

Figure 2.4: The $LaBr_3(Ce)$ (Left) and ^3He (Right) detectors in place on the detector platform.

2.1.4 Detectors

Neither γ-rays nor neutrons are easy to detect as they have no electric charge. In order to detect the thermal neutrons and γ-rays, two very different types of detectors had to be employed. These included a $LaBr_3(Ce)$ scintillator detector for the high-energy γ-rays and a ^3He-based proportional counter for thermal neutrons.

$LaBr_3(Ce)$ γ-ray Scintillator Detector

γ-rays are uncharged and massless elementary particles which interact preferentially with atomic electrons. The $LaBr_3$ crystal is a Cerium (Ce) activated inorganic scintillator. The $LaBr_3(Ce)$ detector is composed of 90-95% $LaBr_3$ and 5-10% $CeBr_3$ [4]. The main mechanism of a scintillator is to produce detectable light from the incoming γ-rays. The incoming γ-rays interact with the electrons of the $LaBr_3(Ce)$ crystal to produce this visible

light. The light is collected by a Photomultiplier tube (PMT) which produces an electrical pulse with characteristics proportional to the energy of the incident γ-ray [5]. Figure 2.5 shows an overview of a scintillator detector.

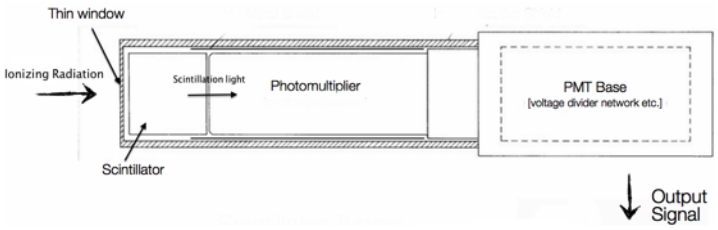

Figure 2.5: Illustration of the different parts of a scintillation detector [2].

The $LaBr_3(Ce)$ detector spectrum has one expected peak at 4.44 MeV caused by the de-excitation of $^{12}C^*$ shown in Eq. 2.1. γ-rays can undergo pair production[3] and produce a electron-positron pair. The positron can then annihilate with an atomic electron in the detector to produce two 511 keV γ-rays. These γ-rays can either be absorbed by the detector or they can escape without interaction or some combination thereof. First- or second-escape peaks occur when one or both γ-rays escape [6]. The resulting peak energies are summarized in Table 2.1.

Peak	Energy (MeV)
Full Absorption	4.44
1st Escape	3.93
2nd Escape	3.42

Table 2.1: The expected γ-ray peaks associated with the 4.44 γ-ray coming from the source.

^{3}He-based Neutron Detector

The ^{3}He proportional counter is shown in Fig. 2.4. In order to detect a neutron, nuclear reactions and/or scattering interactions need to be considered. The source radiates fast neutrons which are thermalized in the water of the Aquarium via scattering processes. The thermal neutrons from the source interact with ^{3}He via:

$$n \; + \; {}^3_2\mathrm{He} \rightarrow \; {}^3_1\mathrm{H} \; + p$$

resulting in a Tritium ($^3_1$H) nucleus, also called a triton (t), and a proton (p). The released proton and triton ionize the surrounding ^{3}He particles and together with the applied voltage produce a detectable burst of ionization. The burst of ionization takes the form of an electrical pulse whose amplitude is proportional to the energy deposited by the p and t in the gas [2]. The reaction Q-value is 0.764 MeV and takes the form of kinetic energy split between the p and t according to their masses. The p and t have the energies $E_p = 0.573$ MeV and $E_t = 0.191$ MeV respectively. This results in three anticipated peaks in the thermal-neutron spectrum [5]. There should be peaks at E_p and E_t corresponding to complete deposition of the energies of either of these reaction

[3] A γ-ray above the threshold E_γ=1.022 MeV can spontaneously produce an electron-positron pair with a total kinetic energy of $E_\gamma - 2m_ec^2$. Note that $m_e = m_{\mathrm{positron}} = 0.511$ MeV/c^2.

products in the detector. The third peak occurs at $E_p + E_t = 0.764$ MeV, where the energy of both reaction products is completely deposited in the detector. The peaks are summarized in Table 2.2.

Peak	Energy (MeV)
$t + p$	0.764
p	0.573
t	0.191

Table 2.2: The expected peaks due to thermal-neutron interactions with ^{3}He.

2.1.5 Data-Acquisition System

To acquire data on the γ-ray and thermal-neutron radiation, the detectors were outfitted with a data-acquisition system. The output signal from each detector was pre-amplified and then processed in a shaping amplifier. The final signal was passed to a Multi-Channel Analyzer (MCA) for histogramming. The data-acquisition system is shown in Fig 2.6.

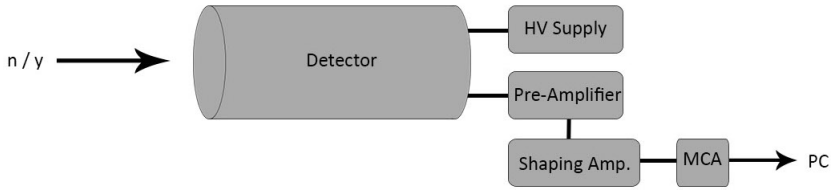

Figure 2.6: The Data-Acquisition System.

Table 2.3 presents the parameters of the data-acquisition system used for the different detectors.

Parameter	$LaBr_3$ (Ce)	^{3}He Tube
Voltage (V)	+600	+1490
Current (μA)	432	0
Gain	20	3
Shaping Time (μs)	0.5	5
Gated Integrator (μs)	0.25	N/A

Table 2.3: Parameters used for the setup of the detectors.

2.1.6 Experimental Procedure

The measurement procedure consisted of performing ten different runs at various positions in the vicinity of the Aquarium aperture as shown in Fig. 2.7. The measurement for the position marked as 12 was performed at a distance of 30 cm from the edge of the aperture to measure background within the room not associated with the source.

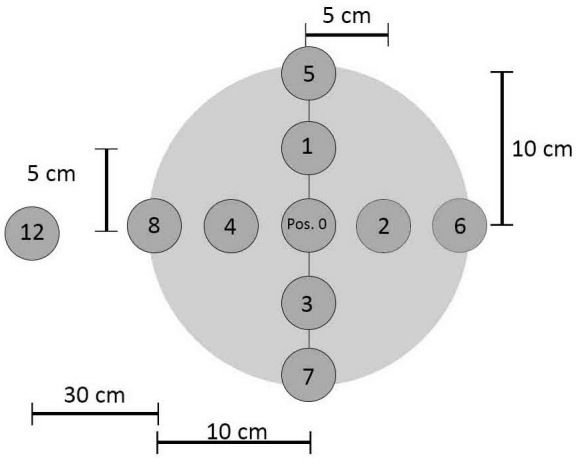

Figure 2.7: The mapping framework lattice.

Chapter 3

Results

3.1 Energy Calibrations

The amplitudes of the electrical pulses from the detectors were registered by the MCA in 8192 bins called ADC (Analog-To-Digital Converter) channels. The pulses are ordered from smallest to largest. The amplitudes of the pulses represent the energy that is deposited in the detector. At this stage, the bins are uncalibrated. In order to understand this spectrum of uncalibrated pulses, each channel must be converted into an energy. By taking the unknown channels and comparing them to energies of known peaks which can be identified in the spectrum, each channel can be mapped to an energy value. In this manner, a function can be derived to convert ADC channels into energies.

3.1.1 $LaBr_3$(Ce) γ-Ray Detector

The $LaBr_3$(Ce) γ-ray detector was calibrated using a variety of γ-ray sources. Along with the known peaks from the Be-based sources, γ-rays from ^{60}Co, ^{137}Cs and ^{22}Na were also used. Other points include the intrinsic activity from ^{138}La and the de-excitation γ-ray of ^{208}Pb* of 2.61 MeV. Table 3.1 lists the sources and γ-rays employed.

Source	E_γ (MeV)	Channel
^{137}Cs	0.662	961 ± 69
^{60}Co	1.17	1612 ± 57
	1.33	1828 ± 50
	2.50	3384 ± 90
^{138}La	1.46	2004 ± 76
^{208}Pb*	2.61	3518 ± 67
PuBe	3.42	4524 ± 91
	3.93	5152 ± 90
	4.44	5757 ± 58

Table 3.1: $LaBr_3$(Ce) γ-Ray Detector Calibration Energies.

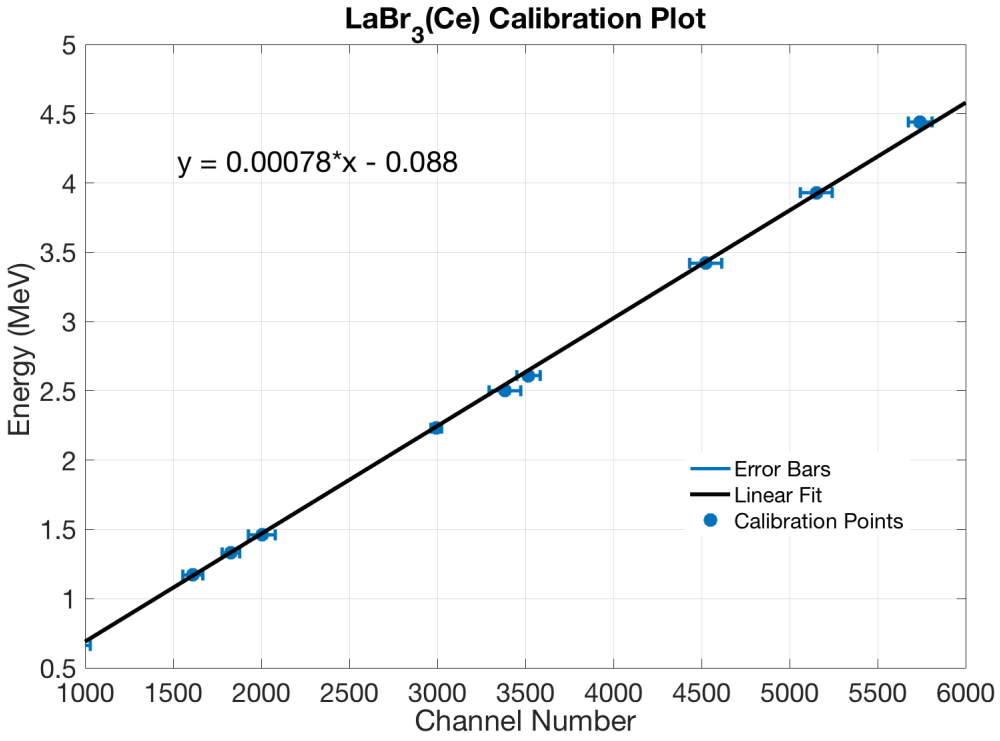

Figure 3.1: $LaBr_3(Ce)$ Calibration Plot.

The visualization of the data from Table 3.1 in Fig. 3.1 indicates the linear nature of these calibration points. The energy of a known γ-ray peak is plotted against the corresponding channel number. A linear fit function is used to map the channel number to energy. Therefore:

$$E_\gamma\,[\text{MeV}] = m \cdot E_\gamma\,[\text{Channel}] + c, \tag{3.1}$$

where m and c are the slope and the offset of the linear function, respectively. Via this relationship, channels may be replaced with energies. The slope is calculated by $m = \frac{\Delta E_\gamma}{\Delta Channel}$. The offset is the intersection of the function with the y-axis. The coefficients in Fig. 3.1 are $m = 0.00078$ MeV/Channel and $c = -0.088$ MeV.

3.1.2 ^{3}He Proportional Counter

The calibration points for the ^{3}He detector are shown in Table 3.2 and are plotted in Fig. 3.2. As can be seen, the response of the ^{3}He proportional counter is linear. Equation 3.2 below is therefore used to calibrate the final measurement data for the ^{3}He detector according to:

$$E_n\,[\text{MeV}] = m \cdot E_n\,[\text{Channel}] + c \tag{3.2}$$

where m and c are the slope and the offset of the linear function, respectively. Via this relationship, channels may be replaced with energies. The coefficients in Fig. 3.2 are $m = 0.00018$ MeV/Channel and $c = 0.12$ MeV.

Peak	E_n (MeV)	Channel
t	0.191	1012 ± 200
p	0.573	3456 ± 239
$t + p$	0.764	4256 ± 153

Table 3.2: ^{3}He Proportional Counter Calibration Energies.

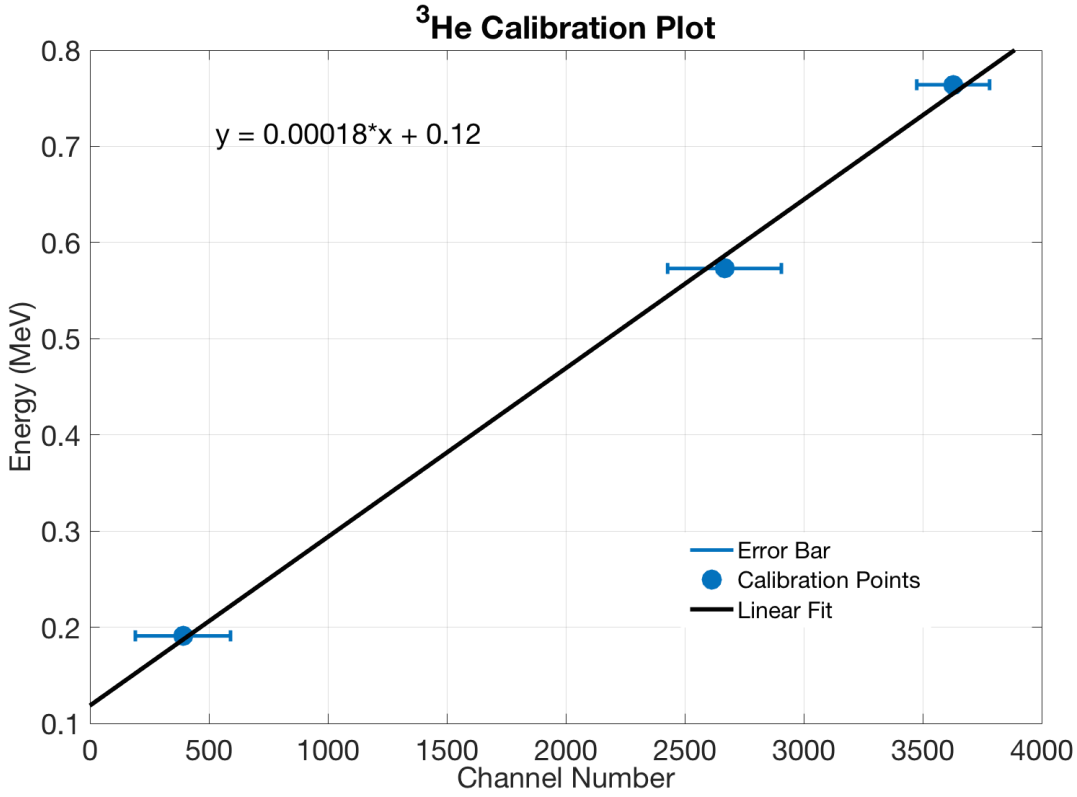

Figure 3.2: ^{3}He Calibration Plot.

3.2 $LaBr_3(Ce)$ γ-Ray Spectra

Figure 3.3 presents the time-normalized γ-ray measurement results obtained with the $LaBr_3(Ce)$ detector corrected for background radiation. Each set of data exhibits essentially the same pattern of peaks. The most distinct peaks in the data arise from a variety of nuclear reactions. The highest energy peak in Fig. 3.3 arises from the decay of $^{12}C^*$ and has the energy 4.44 MeV. The first- and second-escape peaks corresponding to this γ-ray energy have the energies 3.93 MeV and 3.42 MeV, respectively. The region of interest over which this spectrum was integrated to find the background-corrected γ-ray count rates is depicted in Fig. 3.3. This region corresponds entirely to counts associated with the 4.44 MeV γ-ray.

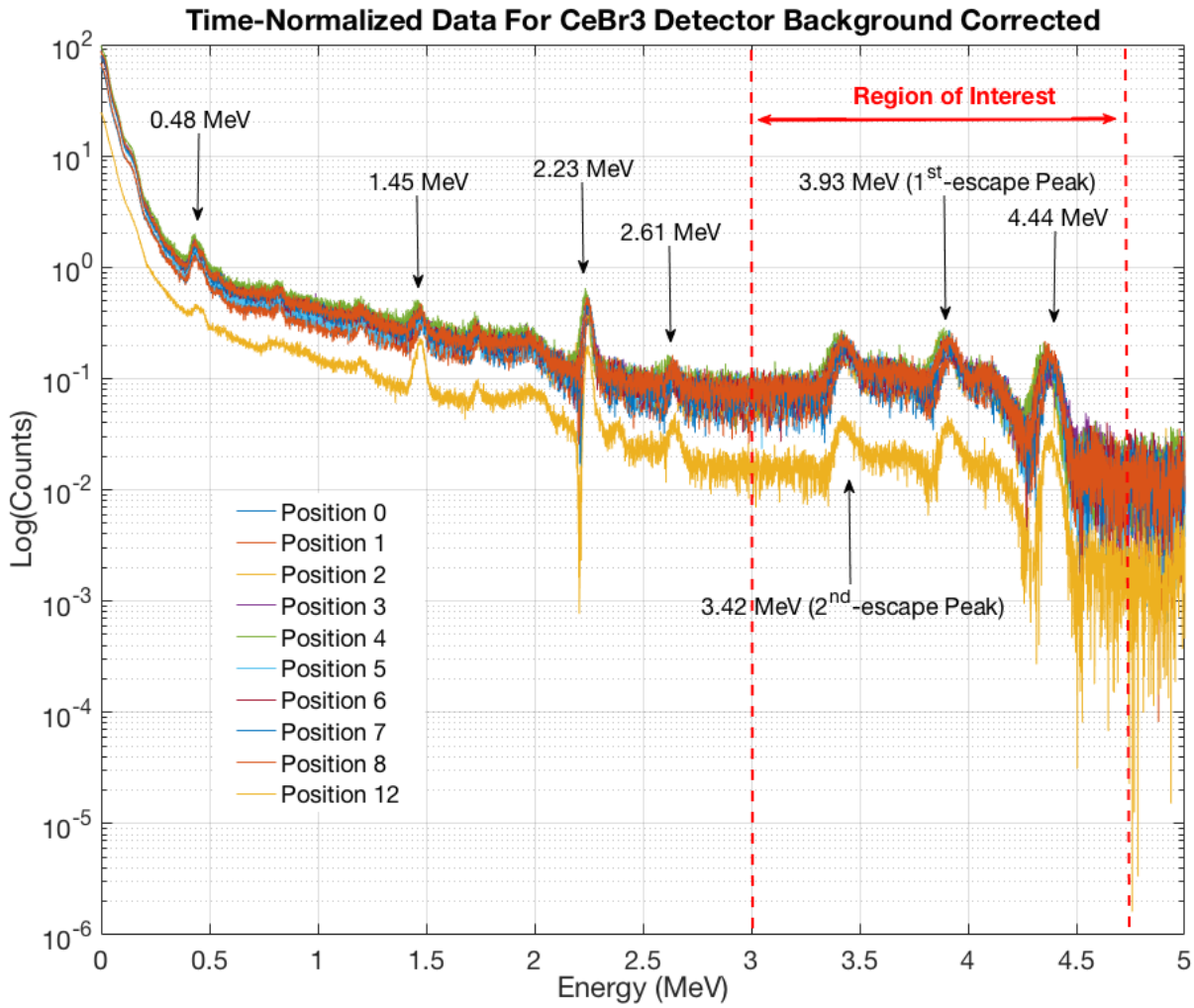

Figure 3.3: γ-ray spectra for all the runs performed, including background measurements. The Region of Interest for the determination of the beam profile is marked.

The origins of the other peaks are explained below.

- the peak at 2.61 MeV comes from the de-excitation of ^{208}Pb* which is present in the concrete walls of the cave in the STF. It is the last step of the 10 generation Thorium chain: ... $^{208}\mathrm{Ti} \rightarrow e^- + \bar{\nu}_e + ^{208}\mathrm{Pb}^* \rightarrow {}^{208}\mathrm{Pb} + \gamma$ (2.61 MeV).
- The peak at 2.23 MeV corresponds to neutron capture by ^{1}H in the water of the Aquarium: $n + {}^1\mathrm{H} \rightarrow {}^2\mathrm{H} + \gamma$ (2.23 MeV).
- The peak at 1.45 MeV corresponds to the intrinsic activity of ^{138}La of the $LaBr_3$(Ce) detector due to electron capture:
  $e^- + {}^{138}\mathrm{La} \rightarrow {}^{138}\mathrm{Ba}^* \rightarrow {}^{138}\mathrm{Ba} + \gamma$ (1.45 MeV).
- The peak at 0.48 MeV originates from neutron capture in ^{10}B found in various borated plastic items: $^{10}\mathrm{B} + n \rightarrow {}^7\mathrm{Li}^* + {}^4\mathrm{He} \rightarrow {}^7\mathrm{Li} + {}^4\mathrm{He} + \gamma$ (0.48 MeV).

3.3 ^{3}He Thermal-Neutron Spectra

Figure 3.4 presents the measurement results obtained with the ^{3}He detector. The data have been time normalized and corrected for background. The entire graph represents the Region of Interest used for the determination of the thermal-neutron beam profile. The full-energy peak and wall-effect shoulders at 0.764, 0.573 and 0.191 MeV can clearly be seen.

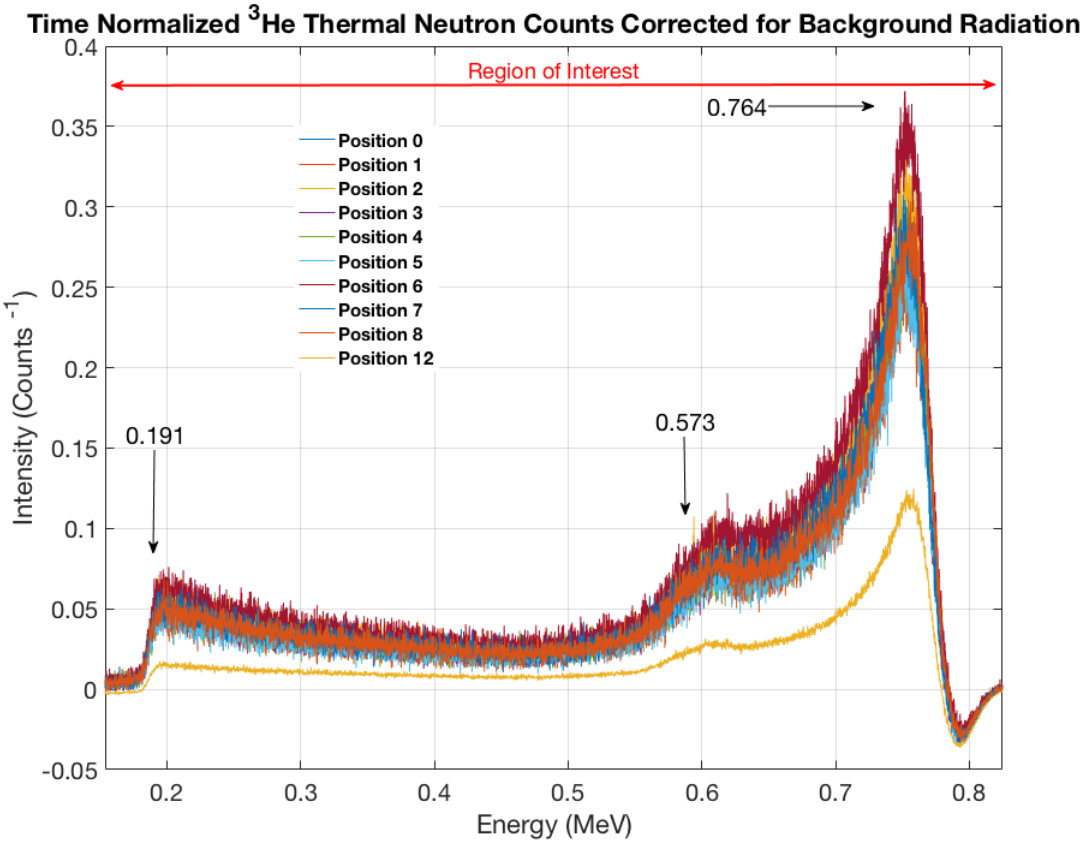

Figure 3.4: The thermal-neutron spectra obtained with the ^{3}He proportional counter together with the marked region of interest for the determination of the beam profile indicated.

3.4 Background-Corrected Count Rates

Table 3.3 presents the time-normalized, background-corrected count rates measured for the $LaBr_3(Ce)$ and ^{3}He detectors at the various positions. These rates were determined by integrating over the Regions of Interest for the γ-ray and thermal-neutron spectra illustrated in Figs. 3.3 and 3.4, respectively.

Position	$LaBr_3(Ce)$ (Counts s^{-1})	^3He (Counts s^{-1})
0	156.039±0.563	195.408±0.363
1	159.966±0.577	180.043±0.345
2	203.270±0.734	199.037±0.394
3	198.968±0.725	230.355±0.366
4	223.845±0.799	197.558±0.365
5	194.159±0.698	180.907±0.350
6	196.133±0.715	208.053±0.416
7	194.751±0.711	256.447±0.374
8	208.805±0.741	206.381±0.367
12	34.815±0.131	70.573±0.079

Table 3.3: Background-corrected count rates.

3.5 Visualization

In this section, visualizations of the background-corrected count rates are presented.

3.5.1 γ-Ray Map

Figures 3.5 and 3.6 show the background-corrected horizontal and vertical γ-ray count rates, respectively. Figure 3.5 illustrates the count rates if you face the aperture as you move left to right, where -40 cm is the leftmost position.

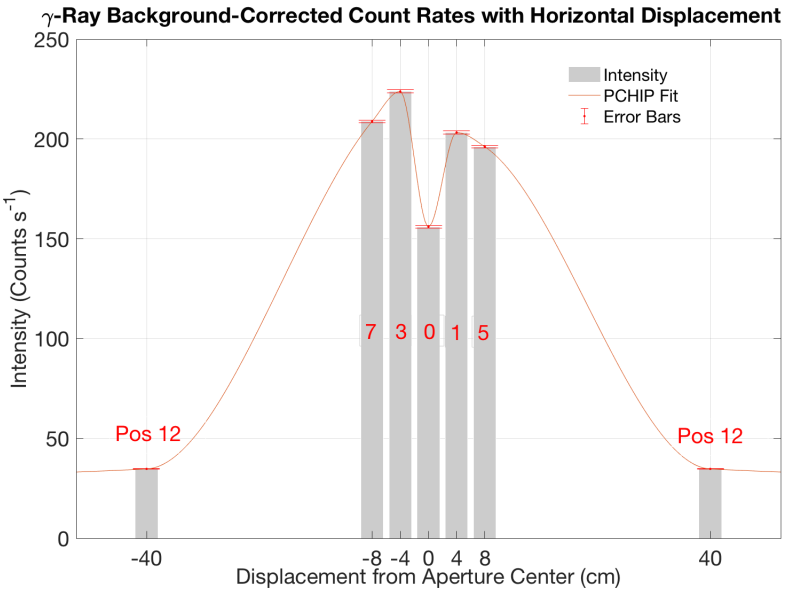

Figure 3.5: The variation of background-corrected γ-ray count rates with horizontal displacement. The origin of the coordinate system is the center of the aperture.

The distribution of results shown in Fig. 3.5 is essentially symmetric around the origin. Figure 3.6 illustrates the count rates from the same location as you move from the floor up, where the lowest point under the aperture is at -40 cm.

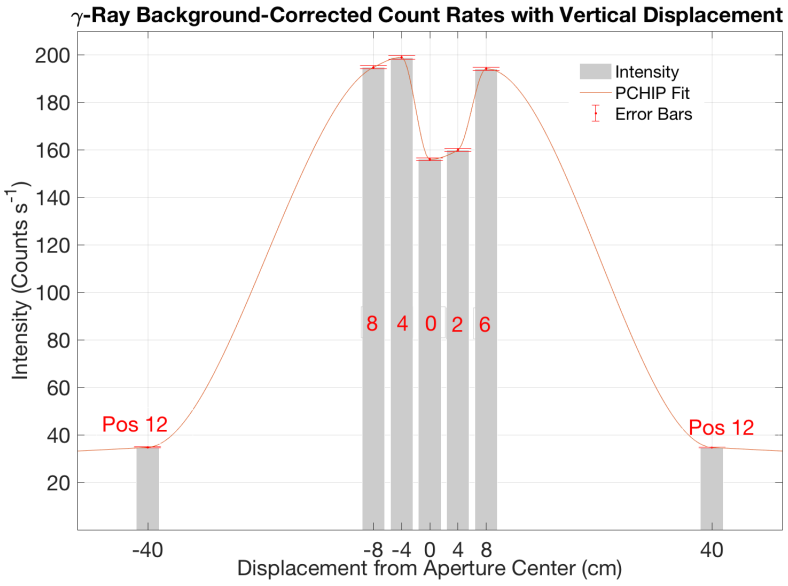

Figure 3.6: The variation of background-corrected γ-ray count rates with vertical displacement. The origin of the coordinate system is the center of the aperture.

The distribution of results shown in Fig. 3.6 is again essentially symmetric around the origin.
A radial function was then determined. The displacement r was defined using

$$r = \sqrt{x^2 + y^2}, \tag{3.3}$$

where x and y are the horizontal and vertical displacement from the center of the aperture, respectively. Figure 3.7 shows the average background-corrected γ-ray count rates at a distance r from the center of the aperture together with a Gaussian fit function.

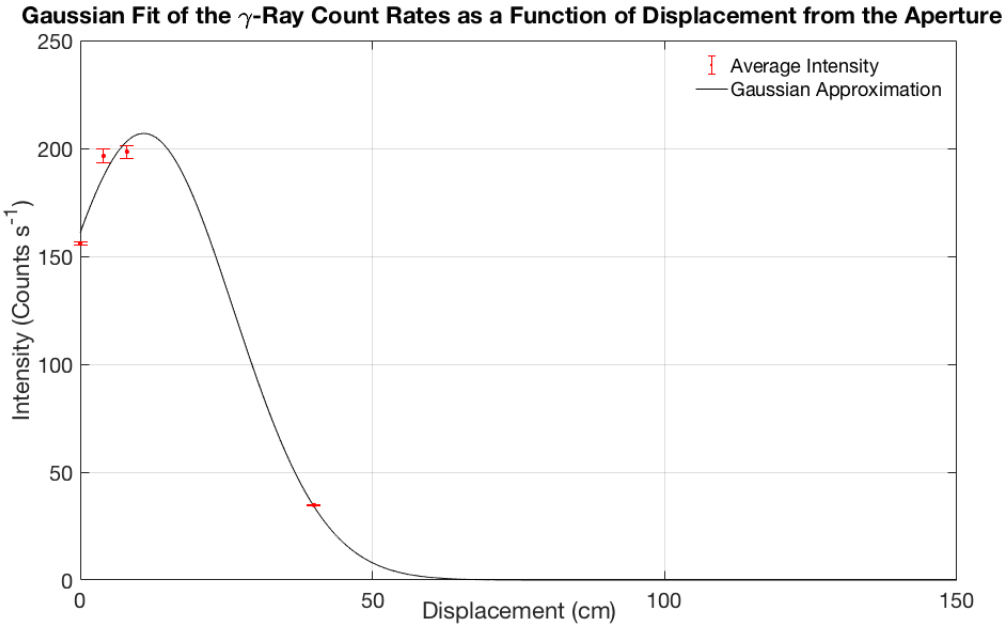

Figure 3.7: Plot of the background-corrected γ-ray count rates as a function of displacement together with a Gaussian fit.

Figure 3.8 shows a 3D visualization of the fitted function determined in Fig. 3.7.

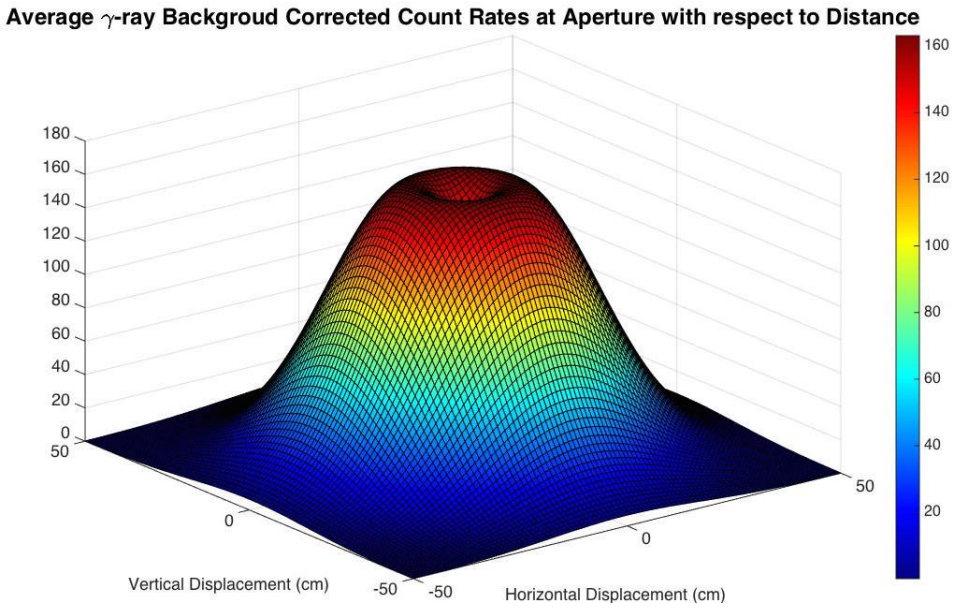

Figure 3.8: Surface plot of the background-corrected γ-ray count rates around the Aquarium aperture. The vertical axis and the colorbar are in units of counts per second.

It can be observed that the background-corrected γ-ray count rates have a dip at the central position.

3.5.2 ^{3}He Map

Figures 3.9 and 3.10 show the background-corrected horizontal and vertical thermal-neutron count rates, respectively.

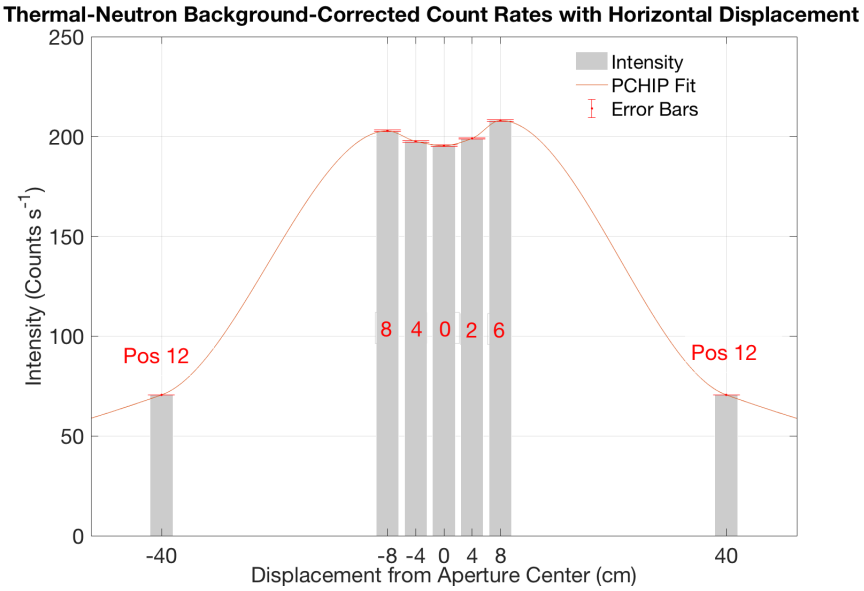

Figure 3.9: The variation of background-corrected thermal-neutron count rates with horizontal displacement from the center of the aperture.

Figure 3.9 illustrates the count rates if you face the aperture as you move left to right, where -40 cm is the leftmost position. The distribution of results in Fig. 3.9 is essentially symmetric around the origin.

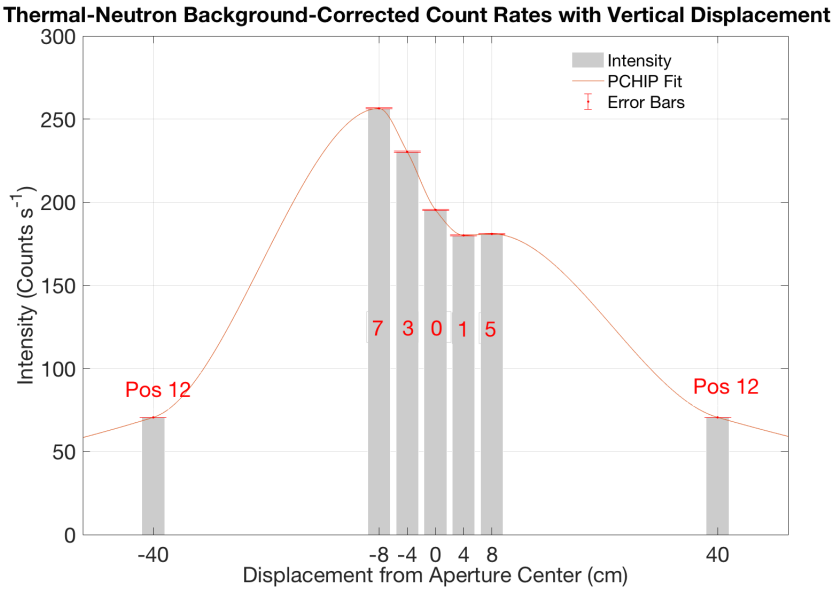

Figure 3.10: The variation of background-corrected thermal-neutron count rates with vertical displacement from the center of the aperture.

Figure 3.10 illustrates the count rates from the same location as you move from the bottom to the top, where -40 cm is the lowest position. Fig. 3.10 reveals an asymmetry in the results. The background-corrected count rates decrease as you move from the bottom position (position 7) to the top of the aperture (position 5).

Despite this asymmetry, and solely for the purpose of visualization, a radial distribution of the data was again determined. In Fig. 3.11, a Gaussian function was fitted to the average background-corrected count rates as a function of the displacement r as detailed previously.

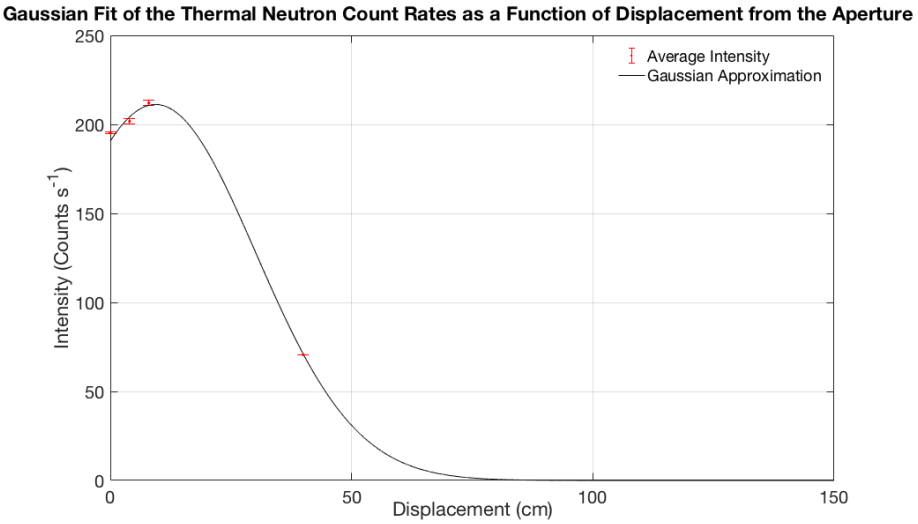

Figure 3.11: Plot of the background-corrected thermal-neutron count rates as a function of displacement together with a Gaussian fit.

Figure 3.12 shows a 3D visualization of the fitted function determined in Fig. 3.11.

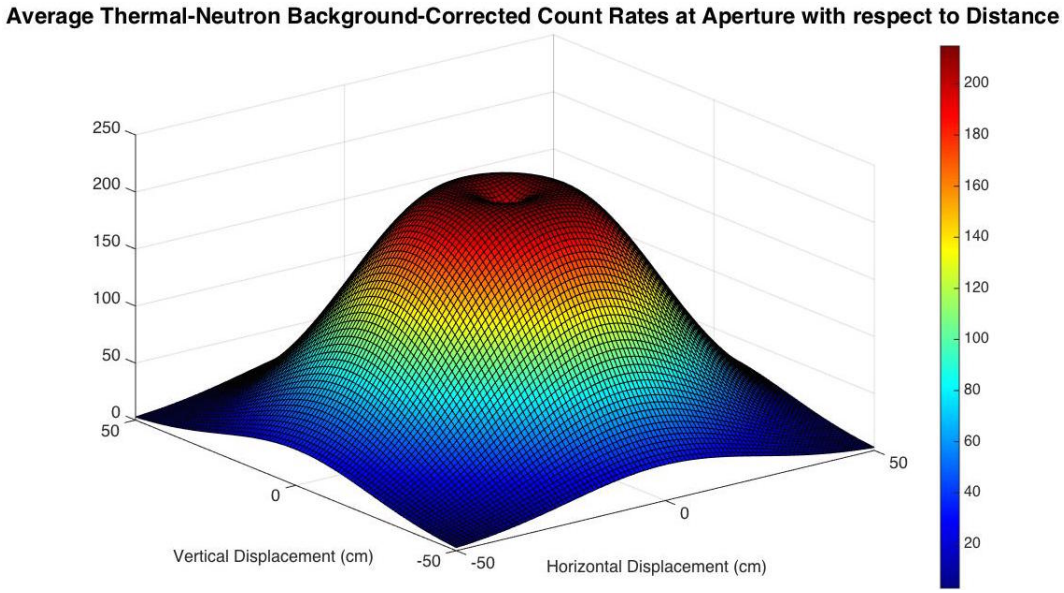

Figure 3.12: Surface plot of the thermal-neutron background-corrected count rates around the Aquarium aperture. The vertical axis and the colorbar are in units of counts per second.

Similar to the background-corrected γ-ray count rates, it can be observed that the background-corrected thermal-neutron count rates have a dip at the central position.

Chapter 4

Discussion & Summary

4.1 Discussion

4.1.1 Consideration of Background Radiation

Accounting for background radiation was crucial to obtaining accurate results. The interlocked area at the STF was home to two Be-based sources at the time of the measurements: a PuBe source in the Aquarium and an Americium-Beryllium source (AmBe) at the back of the room. It was therefore necessary to compensate for the radiation emitted by the AmBe by taking measurements without the PuBe in the interlocked area. The PuBe source was placed inside a shielded barrel and moved to a place remote from the room. The contribution of the AmBe was then measured and subtracted from the primary results. The contribution of the AmBe to the γ-ray results was small as expected. The contribution of the AmBe to the thermal-neutron results was not small (as expected) and may have resulted in the asymmetry in the data.

4.1.2 Central Intensity Dips

From the results of the $LaBr_3$ and ^3He detectors, it is clear that there is a distinct decrease in background-corrected count rates at the center of the Aquarium aperture. This may be due to the fact that the Aquarium tunnel acts as a waveguide for the radiation coming from the source. Relatively fewer γ-rays and thermal neutrons move in a straight line directly from the source to the detector. Relatively more scatter from the tunnel walls. This effect is depicted in Fig. 4.1.

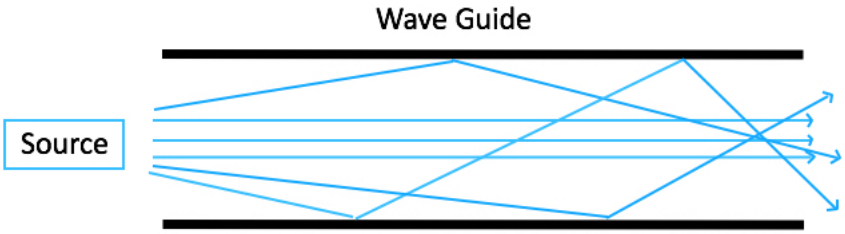

Figure 4.1: An illustration of how radiation may be guided by the Aquarium tunnel to the aperture.

The result is that as you move away from the center of the aperture, the background-

corrected count rate of the radiation field peaks at a distance of ∼5 cm. This is in qualitative agreement with most of the background-corrected count rates.

4.1.3 Thermal-Neutron Count-Rate Asymmetry

As shown in the previous chapter, the shapes of the results obtained using the $LaBr_3(Ce)$ and ^3He detectors are similar. However, there appears an asymmetry in the thermal-neutron count rates varying with vertical displacement for the ^3He detector. In Fig. 3.9, there is a large difference between results obtained at the bottom positions (3 and 7) and the top positions (1 and 5). An explanation for this may be the positioning of four YAP detectors which are in the Aquarium. The position of the YAP detectors is shown in Fig. 4.2. There are clearly YAP detectors between the camera and the source. This means that the YAP detectors can "screen" the thermal-neutron detector resulting in a "shadowing" effect. As result, fewer thermal neutrons will be measured, as fewer can strike the ^3He detector. The data in Fig. 3.10 suggest that the YAP detectors interfere much less with the radiation going to the bottom positions at the Aquarium aperture. This explanation needs further investigation.

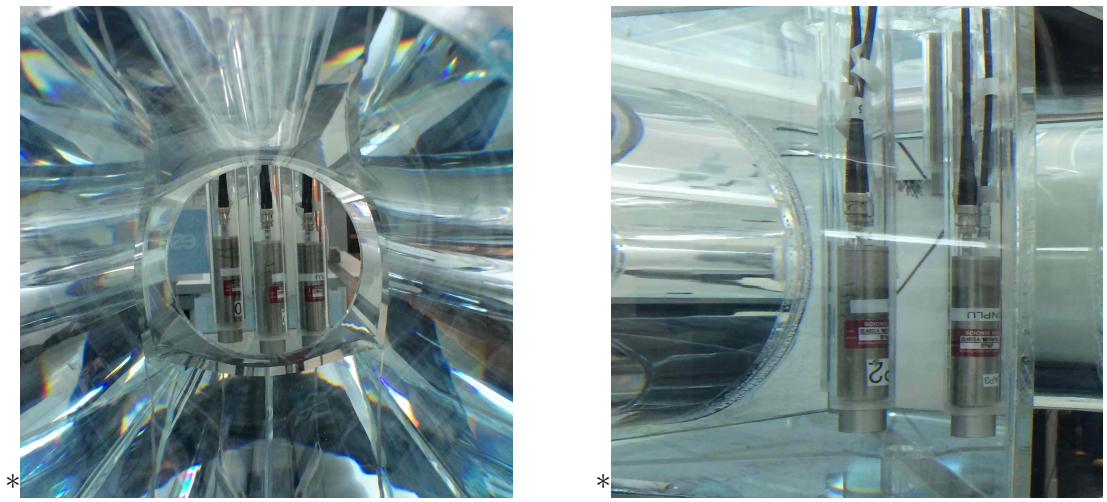

Figure 4.2: The tunnel of the Aquarium with the YAP detectors (left) and the Side-view of the YAP detectors (right).

4.1.4 Accuracy of the Results

The data were measured in two dimensions. Since the data were obtained as shown in Fig. 2.7, many areas of the aperture remain unexplored. To obtain more accurate distributions within and around the proximity of the aperture, more measurements would be desirable. In particular, a lattice of background measurements would provide additional valuable information.

4.2 Summary

The purpose of this thesis was to investigate the radiation emitted by a Be-based source at one of the Aquarium apertures at the STF. γ-ray and thermal-neutron beams were studied. Results for the 4.44 MeV γ-rays and thermal neutrons are reported.

4.2.1 4.44 MeV γ-Rays

The results for the γ-rays show that there is a slight increase in background-corrected count rates as you move outwards radially from the central position of the Aquarium aperture. These rates then quickly tail off, and as you continue to move beyond the edge of the aperture, the background-corrected count rates decrease very rapidly. The horizontal and vertical background-corrected γ-ray count rates demonstrate cylindrical symmetry about the central trajectory through the aperture.

4.2.2 Thermal Neutrons

The thermal-neutron count rates did not demonstrate cylindrical symmetry about the central trajectory through the aperture. The background-corrected thermal-neutron count rates are symmetric in x but asymmetric in y. The background-corrected count rates in y decrease when moving from the lowest position at the aperture to the top position at the aperture. These results were not expected. Further work is needed.

4.2.3 Error Propagation: Results

The particle count rates are given by the following equation:

$$R = \frac{N(\pm\sigma_N)}{T(\pm\sigma_T)} \tag{4.1}$$

where N is the total number of counts, T is the time of measurement (seconds), and σ_N and σ_T are the uncertainties in the values. The standard deviation for the total counts is given by $\sigma_N = \sqrt{N}$ and $\sigma_T = 10^{-3}$ s since this is the least significant digit in the measurement time for the MCA. The standard deviation for the count rate is given by:

$$\sigma_R = \sqrt{\left(\frac{\partial R}{\partial N}\right)^2 \cdot \sigma_N^2 + \left(\frac{\partial R}{\partial T}\right)^2 \cdot \sigma_T^2} = \sqrt{\left(\frac{1}{T}\right)^2 \cdot \sigma_N^2 + \left(-\frac{N}{T^2}\right)^2 \cdot \sigma_T^2} \tag{4.2}$$

Inserting the total number of counts N and the measuring times T gives the standard deviation in the rate. Alternatively, this can be simplified by dividing both sides by the rate R:

$$\frac{\sigma_R}{R} = \sqrt{\left(\frac{\sigma_N}{N}\right)^2 + \left(\frac{\sigma_T}{T}\right)^2} \tag{4.3}$$

Since the term $\left(\frac{\sigma_T}{T}\right)^2$ is negligible to $\left(\frac{\sigma_N}{N}\right)^2$, the standard error of the measurement can be expressed as:

$$\sigma_R \approx R \cdot \frac{\sqrt{N}}{N} \tag{4.4}$$

Error Propagation Example

As an example, the standard deviation in the rate σ_R will be calculated for the γ-ray count rate at position 6 at the aperture. Integrating across the region of interest shown in Fig. 3.3, the total number of counts is $N = 79\,027$ and the time of measurement is $T = 393.098$ s. The input uncertainties are $\sigma_N = \sqrt{79\,027} = 281.117$ and $\sigma_T = 10^{-3}$ for the total counts and the measuring time respectively. Using Eq. 4.2 we find:

$${\sigma_R}^2 = \frac{1}{(393.098\text{ s})^2} \cdot 281.117^2 + \frac{79\,027^2}{(393.098\text{ s})^4} \cdot 10^{-6} = 0.511$$

$$\sigma_R = \sqrt{0.511} = 0.715$$

Using equation 4.4 where $R = 196.805$ and $N = 79\,027$:

$$\sigma_R \approx \frac{196.133}{\sqrt{79\,027}} = 0.697$$

so that $R = 196.1 \pm 0.7$ Counts s^{-1}.

4.2.4 Suggestions for Improvement

In performing the work reported on in this thesis, it became clear that there is definite room for improvement. My suggestions include the following:

1. The ^{3}He detector has a shield made out of ^{10}B which absorbs thermal neutrons. It could have been used to reduce the influence from outside sources of radiation and better define the thermal neutron beam.

2. A lot more measurements could have been performed, i.e. a more comprehensive lattice than that shown in Fig. 2.7 could have been obtained. This applies to both foreground and background measurements.

3. The YAP detectors should have been removed from the Aquarium as they were not used.

4. All the sources in the interlocked area except for the PuBe source could have been removed while making measurements for cleaner results.

Bibliography

[1] K. Fissum, "Measurements with the Primary Aquarium Source." (Private Communication), 2014.

[2] S. Koufigar, "The Radiological Footprint of a Be-Based Neutron Source." http://lup.lub.lu.se/luur/download?func=downloadFile&recordOId=8083315&fileOId=8083334, 2015. (and the references therein).

[3] J. Scherzinger, "Neutron Irradiation Techniques." http://lup.lub.lu.se/record/d4c447d5-ee52-49a9-ad55-4669aed57e32, 2016. (and the references therein).

[4] *Material Safety Data Sheet: Lanthanum Bromide Crystal, Cerium Doped (Brand Name: BrilLanCe^{TM} 380.*

[5] G. F. Knoll, *Radiation Detection and Measurement*. John Wiley & Sons, 2010.

[6] K. S. Krane and D. Halliday, *Introductory Nuclear Physics*, vol. 465. Wiley New York, 1988.

[7] "The Statistics and the Treatment of Experimental Data." https://ned.ipac.caltech.edu/level5/Leo/Stats2_3.html.

Appendix A

Contribution of the Author

Week	Activity
36	Familiarization with STF
37	Familiarization with STF
43	Building Detector Platform
44	Performing $LaBr_3$(Ce) Measurements
45	Performing $LaBr_3$(Ce) Measurements
46	Performing ^{3}He Measurements
47	Performing ^{3}He Measurements
48	Report Writing
49	Report Writing
50	Report Writing

Table A.1: Summary of the contribution of the author week-by-week.

Appendix B

Self-reflection

During this fall term, I have been involved in the work presented in this thesis. The aim was to produce a two-dimensional map of the radiation field of an aperture of the Aquarium at the STF. ^{3}He thermal-neutron and $CeBr_3$ γ-ray detectors were employed. Although I had already acquired theoretical knowledge and some practical experience in the field from previous courses, working on this thesis proved that I knew much less than I thought. I gained a lot of hands-on experience with using equipment, operating particle detectors and how to analyze and interpret recorded data. During the measurements we encountered speed bumps which were eventually overcome. Thanks to the patience and support of my supervisors Kevin and Francesco and the rest of the group, it became an educational, insightful and overall great experience. I feel that I have completed my bachelor's degree with an excellent finish by having chosen to do this thesis.

Appendix C

Error Propagation: Calibration

C.1 γ-Ray Calibration Points

The channel number and its error corresponding to each known energy in Table 3.1 is approximated by fitting a Gaussian function to the known peak. The peak position yields the channel number (x). The standard deviation (σ) measures the variation between values in a data set. The standard deviation is related to the Full Width Half Maximum (FWHM), i.e. the width of the curve at half the peak's amplitude, through the following relation:

$$FWHM \approx 2.355\sigma$$

The value of the channel number is assumed to be $\mathrm{CH}_{\#} \pm \sigma_{CH}$. The standard deviations for each point are reflected by the error bars in the plots in the results. Figure C.1 depicts a Gaussian distribution.

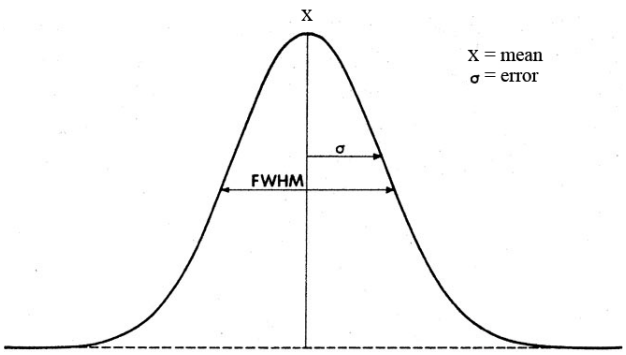

Figure C.1: A gaussian distribution curve. [7]

C.2 Thermal Neutron Calibration Points

This process is repeated for the thermal neutrons. The peak at 0.764 MeV in Fig. 3.4 is fitted to a gaussian to determine the uncertainty. However, the channels for $E_t = 0.191$ MeV and $E_p = 0.573$ MeV hard to determine since the spectrum is not ideal such as that shown in Fig. C.2.

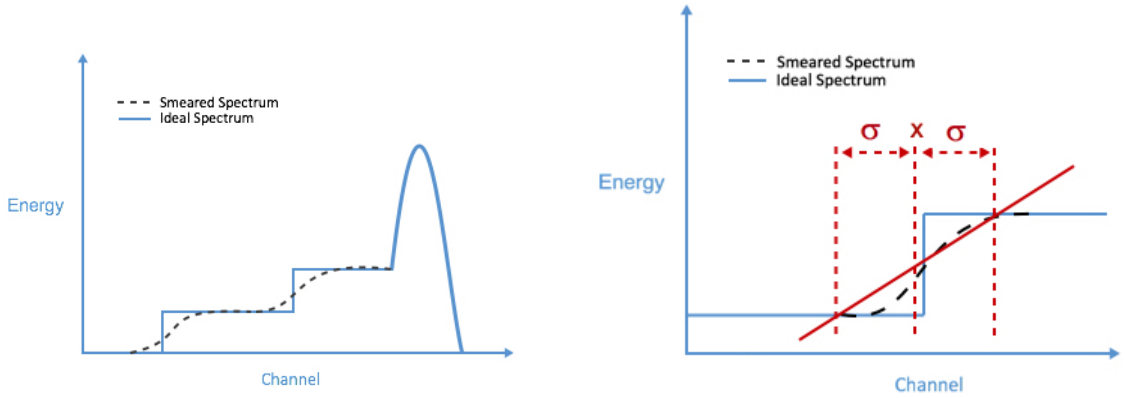

Figure C.2: Ideal vs. Smeared Thermal-Neutron Spectrum (Left). Linear fit to find channel number x and the corresponding error σ (Right).

Figure C.2 shows the ideal ^{3}He curve compared to the real "smeared" spectrum in 3.4. A linear fit is made between the bottom and top of these "shoulders", where the center of the line of best fit corresponds to the expected channel number. The linear fit is shown in Fig. C.2 as well as the derivation of the error term σ.

The project reported upon in this thesis
was performed in collaboration with

The Source-based Neutron Irradiation Group
of the Division of Nuclear Physics at Lund University

and the

The Detector Group of the European Spallation Source